AIP | Journal of Applied Physics

Structural conditions that leads to photoluminescence emission in SrTiO3: An experimental and theoretical approach

V. M. Longo, A. T. de Figueiredo, S. de Lázaro, M. F. Gurgel, M. G. Costa et al.

Citation: J. Appl. Phys. **104**, 023515 (2008); doi: 10.1063/1.2956741
View online: http://dx.doi.org/10.1063/1.2956741
View Table of Contents: http://jap.aip.org/resource/1/JAPIAU/v104/i2
Published by the AIP Publishing LLC.

Structural conditions that leads to photoluminescence emission in $SrTiO_3$: An experimental and theoretical approach

V. M. Longo,[1,a)] A. T. de Figueiredo,[1] S. de Lázaro,[1] M. F. Gurgel,[1] M. G. S. Costa,[2] C. O. Paiva-Santos,[2] J. A. Varela,[2] E. Longo,[2] V. R. Mastelaro,[3] F. S. DE Vicente,[3] A. C. Hernandes,[3] and R. W. A. Franco[4]
[1]*LIEC, Departamento de Ciências e Engenharia de Materiais e Departamento de Química, UFSCar, P.O. Box 676, São Carlos, Sao Paulo 13565-905, Brazil*
[2]*LIEC, Instituto de Química, UNESP, P.O. Box 355, Araraquara, Sao Paulo 14801-970, Brazil*
[3]*Instituto de Física de São Carlos, USP, P.O. Box 369, São Carlos, Sao Paulo 13560-970, Brazil*
[4]*Centro de Ciências e Tecnologia, UENF, Campos dos Goytacazes, Rio de Janeiro 28013-602, Brazil*

(Received 5 November 2007; accepted 14 May 2008; published online 21 July 2008)

Complex cluster $[TiO_5 \cdot V_O^z]$ and $[SrO_{11} \cdot V_O^z]$ (where $V_O^z = V_O^X$, $V_O^{\bullet}$, $V_O^{\bullet\bullet}$) vacancies were identified in disordered $SrTiO_3$ powders prepared by the polymeric precursor method, based on experimental measurements by x-ray absorption near edge structure spectroscopy. The paramagnetic complex states of $[TiO_5 \cdot V_O^{\bullet}]$ and $[SrO_{11} \cdot V_O^{\bullet}]$ with unpaired electrons were confirmed by electron paramagnetic resonance spectroscopy. The disordered powders showed strong photoluminescence at room temperature. Structural defects of disordered powders, in terms of band diagram, density of states, and electronic charges, were interpreted using high-level quantum mechanical calculations in the density functional framework. The four periodic models used here were consistent with the experimental data and explained the presence of photoluminescence. © *2008 American Institute of Physics*. [DOI: 10.1063/1.2956741]

I. INTRODUCTION

The development of advanced semiconductor materials with wide band gaps (2.0–4.0 eV) may give rise to new optoelectronic devices, particularly materials for application in the development of green or blue light-emission diodes or laser in the spectrum of visible light. In many optoelectronic devices, disordered insulators can replace single crystal semiconductors, particularly when cost is an important factor.[1]

$SrTiO_3$ (ST) has a simple cubic perovskite structure and is a semiconductor with an indirect band gap usually ranging from 3.2 to 3.4 eV.[2,3] By modifying ST structurally, this material can be made to show a variety of physical properties. For example, a small amount of electron doping by chemical substitution of oxygen vacancies renders the material conducting and even superconducting at low temperatures.[4,5]

Light doping with electrons ($\sim 10^{19}$ cm^{-3}) makes the originally insulating ST metallic because of significant screening resulting from a nearby ferroelectric instability.[6,7] Such a variety of fascinating physical properties is a strong indication that ST may have uses in the emerging field of oxide-based electronics.

Several authors have reported a greenish emission by pure ST crystals at low temperatures (35 K) (Refs. 8–10) when they are excited by radiation energy above the band gap.[11–13] Investigations into the temperature dependence of visible emission have demonstrated that this emission band is quenched at temperatures above 110 K.

Using time-resolved spectroscopy, Leonelli and Brebner proposed a model to describe the luminescence process in which electrons form small polarons that interact with holes to produce self-trapped excitons (STEs), with the recombination of STEs resulting in visible emission, either immediately subsequent to or sometime after being trapped by impurities and defects.[14,15]

More recently, several phenomena of photoluminescence (PL) at low temperature have been reported in the perovskite-type structure and the effects observed have been ascribed to the recombination of electrons and hole polarons forming a charge transfer vibronic exciton.[16,17]

In nanocrystalline ST, PL has been detected at room temperature and with excitation energies below the energy band gap.[18–21] The visible emission was attributed to STEs and was correlated not only to the intrinsic surface states and defect centers via a strong electron-phonon interaction but also to particle sizes.

Our group demonstrated that a series of structurally disordered titanates ($ATiO_3$, where A=Ca, Sr, and Ba), synthesized by a soft chemical process called the polymeric precursor method, showed intense PL at room temperature when excited by a 488 nm laser excitation line.[22–24] This emission was attributed to localized levels above the valence band (VB) and below the conduction band (CB). Moreover, a charge transfer occurred from the $[TiO_6]$ cluster to the $[TiO_5]$ cluster in the disordered system.[23–26]

After further advances in studies of the electronic transitions that display PL emission, Kan *et al.*[27] concluded that oxygen deficiency in Ar^+-irradiated ST is the only cause for blue-light PL emission at room temperature. However, several reports in the literature explain the favorable conditions for PL emission in materials presenting a degree of order-disorder.[28–30] The authors attributed the radiative decay

[a)]Author to whom correspondence should be addressed. Electronic mail: valerialongo@liec.ufscar.br.

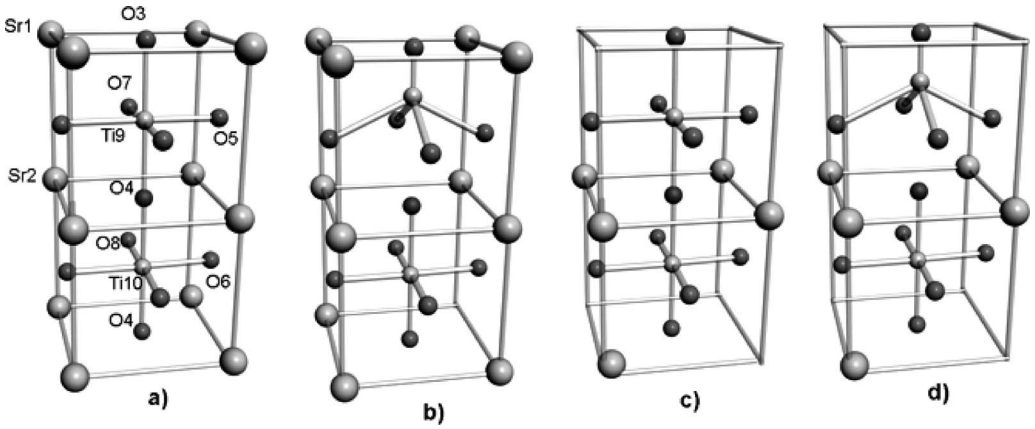

FIG. 1. (a) Ordered model of symmetric ST-o; (b) asymmetric model of network former dislocation, ST-f; (c) asymmetric model of network modifier dislocation, ST-m; and (d) asymmetric model of network former and modifier dislocation, ST-fm.

process to distorted octahedrons,[28] STEs, oxygen vacancies, surface states,[29] and a charge transfer via intrinsic defects inside an oxygen octahedron.[30] As can been seen, there is no general consensus in the literature about *why* and *how* radiative decay takes place in perovskitelike structures with a certain degree of disorder.

PL is an effective tool that provides important information about a material's physical properties at the molecular level, including shallow and deep level defects and gap states in many insulators.[31] Several models have been proposed to explain how these defects influence PL emission. According to the charged dangling bond model, inherent defects, identified as D^+-D^- charged pairs, are formed due to the rearrangement of unpaired spins. In the valence-alternation pair (VAP) model, these defects can be formed close to each other due to Coulomb attraction and are called intimate VAPs (IVAP).[32–34] VAP and IVAP are also known as random and nonrandom defects, respectively.[35] The intrinsic defects discussed above are considered the major contributors to the gap states in insulators.

For a theoretical approach to the experimental PL results of violet, blue, green, yellow, and red light emissions, three types of disorder were simulated in the crystalline (ordered) cubic $1\times1\times2$ supercell, based on experimental x-ray absorption near edge structure (XANES) spectroscopy, as follows: in the network former (Ti), in the network modifier (Sr), and in the network former modifier (Ti/Sr). The purpose of these theoretical simulations was to demonstrate how different structural defects contribute to the disordered system and give rise to specific states in the forbidden gap, leading to different electronic transitions and, hence, to different colored light emissions. On the experimental side, various complementary characterization techniques were used, such as electron paramagnetic resonance (EPR) spectroscopy, optical absorption, and PL spectroscopy, to obtain a clearer picture of the physics underlying the luminescence behavior of ordered and disordered ST perovskite structures.

II. EXPERIMENTAL PROCEDURES

The ST powders studied here resulted from a soft chemical process, the polymeric precursor method.[36] In this method, titanium citrates were formed by the dissolution of titanium isopropoxide in an aqueous solution of citric acid (60–70 °C). After homogenization of the Ti solution, $SrCO_3$ was slowly added. To dissolve the $SrCO_3$ completely, the temperature was kept at 100–110 °C. The complete dissolution of the salts produced a clear solution. After the complete dissolution of the $SrCO_3$ salt, ethylene glycol was added to polymerize the mixed citrates by a polyesterification reaction. The molar ratio of strontium to titanium was 1:1 and the ratio of citric acid to ethylene glycol was set at 60:40 (mass ratio). The polymeric resin was pyrolized at 300 °C for 2 h, resulting in a powder containing organic residues due to the method employed. The heat treatment was then conducted at different temperatures for 2 h, applying a heating rate of 10 °C/min, in a tube furnace under an oxygen flow to promote prepyrolysis and total oxidation of the organic precursor.

The ST powders were structurally characterized by x-ray diffraction (XRD) (Cu $K\alpha$ radiation), and the diffraction patterns were recorded in a Bragg–Brentano diffractometer (Rigaku 2000) at Cu $K\alpha$ in a θ-2θ configuration, using a graphite monochromator. Two kinds of powder must be distinguished for a better understanding of this work: the first, a structurally disordered powder, which was heat treated below the crystallization temperature, and the second, a structurally ordered powder, which reached crystallization. The spectral dependence of the optical absorption of the ordered and disordered powders was measured at room temperature in the total reflection mode, using a Cary 5G UV-vis spectrophotometer. The PL spectra were recorded with a Jarrel-Ash Monospec 27 thermal monochromator and a Hamamatsu R446 photomultiplier. The 350.7 nm exciting wavelength of a krypton ion laser (Coherent Innova) was used, with the laser's nominal output power kept at 200 mW. EPR spectra were recorded with a Varian E-109 spectrometer operating in the *X*-band (9 GHz), at a microwave power of 0.5 mW, and a modulation frequency of 100 kHz. The *g*-factor was referenced with respect to $MgO:Cr^{3+}$ ($g=1.9797$) as the external standard. The EPR spectra were evaluated using the SIMFONIA® program.[37]

XANES spectra at the Ti *K*-edge were measured using the D04B-XAFS1 beam line at the National Laboratory of Synchrotron Light (LNLS) in Campinas, SP, Brazil. The Ti

K-edge data were collected in the transmission mode using a Si (111) channel-cut monochromator. The XANES spectra were measured from 50 below and 200 eV above the edge, with an energy step of 0.3 eV near the edge region. To compare various samples, all the spectra were background removed and normalized using as unity the first EXAFS oscillation.

All the measurements were taken at room temperature (298 K).

III. COMPUTATIONAL METHOD AND PERIODIC MODELS

ST crystallizes in the cubic perovskite structure ($Pm3m$ space group, O_h symmetry). The strontium atoms share the corners of the unit cell and the titanium is at the center of the cube, surrounded by six oxygens that occupy the middle of the faces in a regular octahedral configuration. A $1\times1\times2$ supercell was used as a periodic model to represent the crystalline ordered ST (ST-o), containing ten atoms in the unit cell [see Fig. 1(a)]. This ST-o can be designated $[TiO_6]$–$[TiO_6]$, since each titanium atom is surrounded by six O in an O_h configuration.

The experimental and calculated values of the **a** parameter were 3.91 and 3.88 Å, respectively.[38] The experimental value of the **a** parameter was used to calculate the ordered and disordered structures.

Three models (Fig. 1) were built to simulate the disordered type: (i) displacement of the network former, Ti (ST-f); (ii) displacement in the network modifier, Sr (ST-m); and (iii) simultaneous displacement in the network former modifier, Ti/Sr (ST-fm).

Ab initio calculations were made with the CRYSTAL98 (Ref. 39) package within the framework of the density functional theory (DFT), using the gradient-corrected correlation functional by Lee *et al.* combined with the Becke3 exchange functional, B3LYP,[40,41] which Muscat *et al.*[42] demonstrated to be suitable for calculating structural parameters and band structures in a wide variety of solids. The atomic centers were described by the all-electron basis sets 976-41(d51)G for Sr, 86-411(d31)G for Ti, and 6-31G* for O.[43]

The k-point sampling was chosen to be 40 points within the irreducible part of the Brillouin zone. To simulate the displacement of Ti and Sr atoms, as explained in the next section, we used the ATOMDISP option provided with the CRYSTAL program. The XCRYSDEN program was used to design the density of states (DOS) and the band structure diagrams.[44]

The purpose of this modeling was not to represent the exact reality of disordered structures, but to outline a simple scheme for a better understanding of the effects of structural deformation on the electronic structure without completely suppressing the geometry of the cell, which is useful in periodic calculations.

IV. RESULTS AND DISCUSSION

Figure 2 shows the evolution of the XRD patterns of ST powders heat treated at 673, 723, 773, 823, and 1023 K for 2 h in an oxygen atmosphere. XRD diffraction peaks were

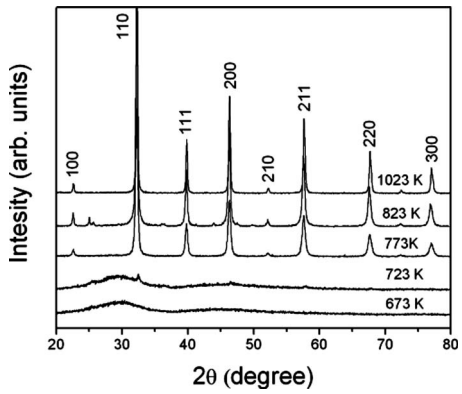

FIG. 2. XRD patterns of five samples of ST powder annealed at 673, 723, 773, 823, and 1023 K for 2 h in an oxygen flow.

observed in powder annealed at 823 and 1023 K, indicating that the samples were structurally ordered in the long range. Moreover, the XRD pattern of the ST annealed at 823 and 1023 K indicated that this material possessed a single phase and could be completely indexed on the basis of the cubic ICDD card no. 35-0734 ($Pm3m$). However, the crystallization process of the structurally disordered ST clearly began at a temperature as low as 773 K (see Fig. 2), and was well ordered after annealing at 823 K.

Figure 3(a) shows the XANES spectra of ST compounds as a function of the annealing temperature, allowing for an accurate assessment of the material's short range order-disorder.

Based on the literature, peak A was caused primarily by the quadrupole excitation of 1s electron to the t_{2g} orbitals of the Ti atom.[45,46] Peak B arose from the excitation of 1s electron to e_g orbitals of the same octahedron and contained both quadrupole and dipole (caused by p-d mixing) contributions. The intensity of the pre-edge peak B has been shown to be sensitive to the short range order around Ti atoms. On the other hand, the pre-edge feature labeled C was shown to be caused by Ti 1s electron transition to the unoccupied 3d-originated e_g-type molecular orbital of $[TiO_6]$ polyhedra neighboring the absorbing Ti atoms, which are weakly affected by the core hole potential.[45]

The XANES spectra can be divided into two groups on the basis of the pre- and postedge features, one with three low intensity peaks and the other with a single intense peak. Feature A corresponds to the 1s-3d (e_g) quadrupolar transition in the titanium atom. Feature B has both a quadrupolar 1s-3d (t_{2g}) component and a dipolar one to a p-like state induced by the hybridization of the 3d states with the p states of the surrounding oxygen. Feature C is due to the neighboring titanium atoms and has a dipolar character. The observation of two types of pre-edge B features strongly suggests that there was a change in the coordination environment of titanium in the ST samples, since the calcination temperature decreased. A similar behavior was observed in the $Ca(Zr_1Ti_{1-x})O_3$ and $CaTiO_3$ compounds as a function of the heat-treatment temperature.[47]

The XANES spectra of ST compounds heat treated at 773, 823, and 1023 K were very similar to those reported in the literature for the crystallized ST compound. The minor

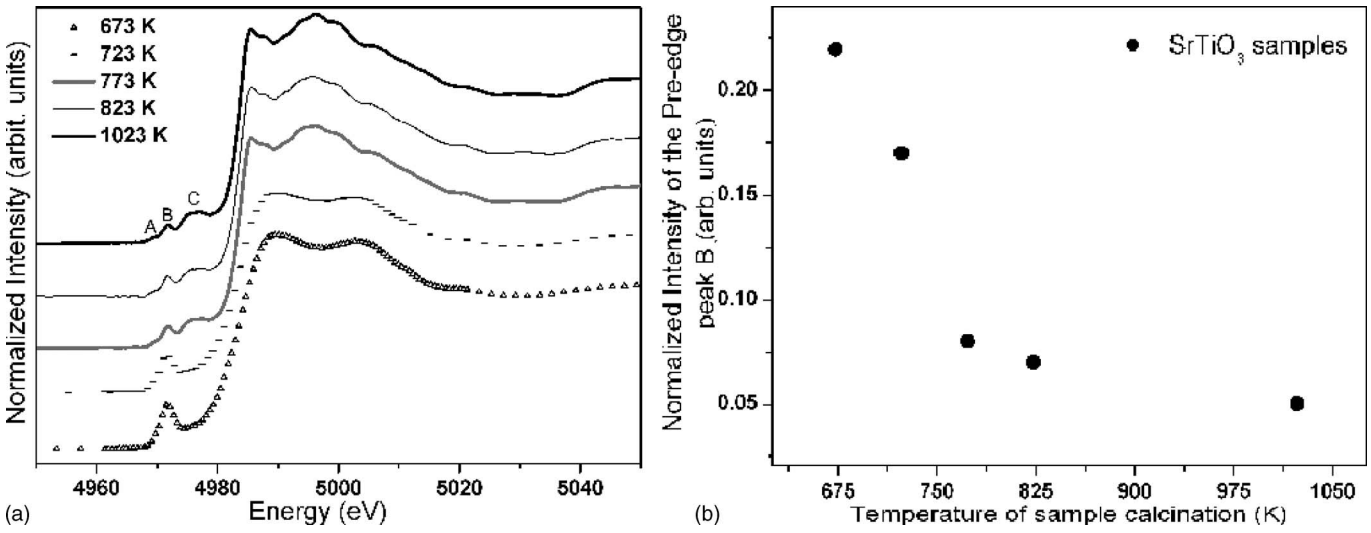

FIG. 3. (a) Ti *K*-edge XANES spectra at room temperature for the ST powder annealed at 673, 723, 773, 823, and 1023 K. (b) Normalized intensity of the pre-edge peak *B* at the same temperatures.

differences observed at the height of the pre-edge peak B were attributed to the fact that, as the temperature increased, the sample became more ordered.[39,48] The pre-edge features observed in these three samples are characteristic of titanium atoms in an approximately centrosymmetric environment.

On the other hand, in line with the literature, the pre-edge B feature of ST compounds heat treated at 673 and 723 K is characteristic of a mixture of fivefold and sixfold coordinated titanium atoms.[47,49] According to the work of Farges *et al.*,[49] titanium atoms in different coordination numbers, $^{[4]}$Ti, $^{[5]}$Ti, and $^{[6]}$Ti, are distinguishable according to their position and height (or intensity) of the pre-edge peak.

Figure 3(b) depicts the variation of the normalized intensity of the pre-edge peak B as a function of the calcination temperature. The intensity of the pre-edge B peak in the 673 and 723 K samples was significantly higher than that of the other samples, indicating the presence of a certain amount of $^{[5]}$Ti atoms. Moreover, for $^{[4]}$Ti, $^{[5]}$Ti, and $^{[6]}$Ti, Farges *et al.*[49] found the areas to be roughly proportional to height, i.e., areas of 1.0–1.2, 0.8, and 0.1–0.6, respectively.

The powders studied here displayed two types of environments for the titanium, namely, a fivefold $[TiO_5]$ square-based pyramid and a sixfold coordination $[TiO_6]$ octahedron. The order can be ascribed to the presence of $[TiO_6]$ clusters, while the increasing disorder can be attributed to the increasing presence of $[TiO_5]$ clusters. The powder annealed at 773 K was short range ordered, but a little disorder still remained in the long-range order, as indicated by the widening of the diffraction peak.

In this context, oxygen vacancies in titanates can occur in three different charge states: the $[TiO_5 \cdot V_O^X]$ complex state, which has two paired $\uparrow\downarrow$ electrons and is neutral relative to the lattice; the singly ionized $[TiO_5 \cdot V_O^{\bullet}]$ complex state, which has one unpaired $\uparrow$ electron; and the $[TiO_5 \cdot V_O^{\bullet\bullet}]$ complex state, which has no unpaired electron and is doubly positively charged in relation to the lattice. Another portion of electrons and holes may be trapped by intrinsic crystal defects in the network modifier complex $[SrO_{11} \cdot V_O^z]$, where $V_O^z = V_O^X$, $V_O^{\bullet}$ or $V_O^{\bullet\bullet}$.

Figure 4 illustrates the spectral dependence of the absorption of the disordered ST annealed at 673, 723, and 773 K and the ordered ST powders annealed at 823 K. The ordered powder presents a well-defined absorption front, while the structurally disordered powders typically exhibit a continuous smooth increase in absorption as a function of the energy, suggesting the presence of localized states inside the band gap. The optical gaps obtained by extrapolation of the linear curve regions according to the Wood and Tauc method[50] were 3.20 for the ordered sample annealed at 823 K and 1.61, 2.25, and 3.09 eV for the disordered powders annealed at 673, 723, and 773 K, respectively. These results indicate that the exponential optical absorption edge and the optical band gap energy are controlled by the degree of structural order-disorder in the lattice of ST powders.

The decrease in the band gap in structurally disordered powder can be attributed to oxygen vacancies, lattice defects, impurities, and/or local bond distortion, which yield localized electronic levels in the band gap of this material. The tail observed in the disordered samples indicated that the presence of complex clusters of $[TiO_5 \cdot V_O^z]/[SrO_{11} \cdot V_O^z]$ cre-

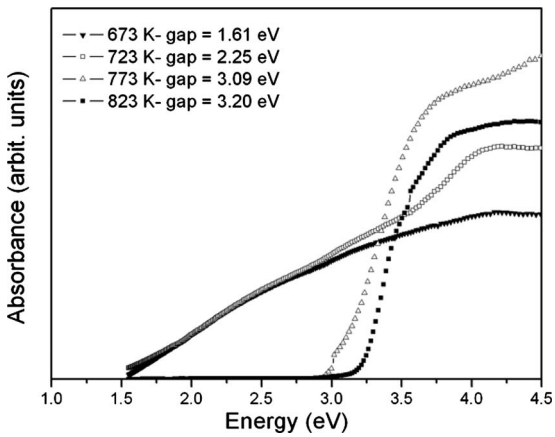

FIG. 4. Spectral dependence of the absorbance of disordered ST annealed at 673, 723, 773 K, and of ordered ST powder annealed at 823 K for 2 h in an oxygen flow.

ated localized electronic levels in the forbidden band gap. With the increasing order of the ST powder, the band gap increased, indicating the reduction of localized electronic states and defects linked to structural disorder. UV-vis is a useful tool for investigating the order-disorder of materials, but it does not indicate the structural disorder to which localized states are connected.

Over the past decade, advances in computational methods and increasing computing power have been made it possible to use first-principles calculations to examine condensed system problems that are difficult to address experimentally.

Thus, based on our experimental XANES findings, a theoretical model was built to represent the network former disordered ST (ST-f) by shifting the titanium 9 by a (0 0 0.2) Å vector from its previous position in the former $1\times1\times2$ supercell. This displacement renders the unit cell asymmetric, with Ti9 now surrounded by five oxygen atoms in a square-based pyramid configuration, while Ti10 is surrounded by the remaining six oxygen atoms, as in the case of ST-o. Therefore, this asymmetric ST model, ST-f, represents the disorder in the network former material. This structure can be expressed as $[TiO_6]$–$[TiO_5\cdot V_O^z]$ [see Fig. 1(b)]. This explanation of vector displacement takes into account previous work on the perovskite structure.[23,24]

Recently, Lazaro *et al.*[51] reported results of a pre-edge feature of Ti and Ca *K*-edge XANES in a disordered $CaTiO_3$ perovskitelike structure. Their findings indicated two types of environments for the calcium, namely, 11-fold and 12-fold calcium coordinations. Based on this information, the network modifier disorder (ST-m) was modeled by shifting the strontium 1 by a (0.12 0.12 0.12) Å vector from its previous position in the modifier $1\times1\times2$ supercell. This displacement produces asymmetries in the unit cell, with the Sr1 now surrounded by 11 oxygen atoms and Sr2 surrounded by 12 oxygen atoms, as in the case of ST-o. Therefore, this asymmetric ST model, ST-m, represents the disorder in the network modifier material. This structure can be called $[SrO_{12}]$–$[SrO_{11}\cdot V_O^z]$ [see Fig. 1(c)]. This vector displacement direction was chosen based on the work of Stern,[52] who stated that the order-disorder component of phase transitions in $BaTiO_3$ consists of local displacements from a cubic symmetry, causing partial loss of long-range correlations but remaining constant in magnitude across phase transitions, while the displacive component is a reorientation of the local displacements relative to the (111) directions as the disorder increases.

Lastly, the network former and modifier disorder (ST-fm) were modeled simultaneously by shifting titanium and strontium atoms, as described above. This displacement caused asymmetries in the unit cell, with the Ti9 now surrounded by five oxygen atoms in a square-based pyramid configuration, Ti10 surrounded by six oxygen atoms, Sr1 surrounded by 11 oxygen atoms, and Sr2 surrounded by 12 oxygen atoms. Therefore, this asymmetric ST model, ST-fm, represents the disorder in network former and modifier material. This structure can be called $[TiO_6]$–$[TiO_5\cdot V_O^z]$ and $[SrO_{12}]$–$[SrO_{11}\cdot V_O^z]$ [see Fig. 1(d)]. With these models, the effects of different structural disorders can be evaluated separately in terms of their electronic structure.

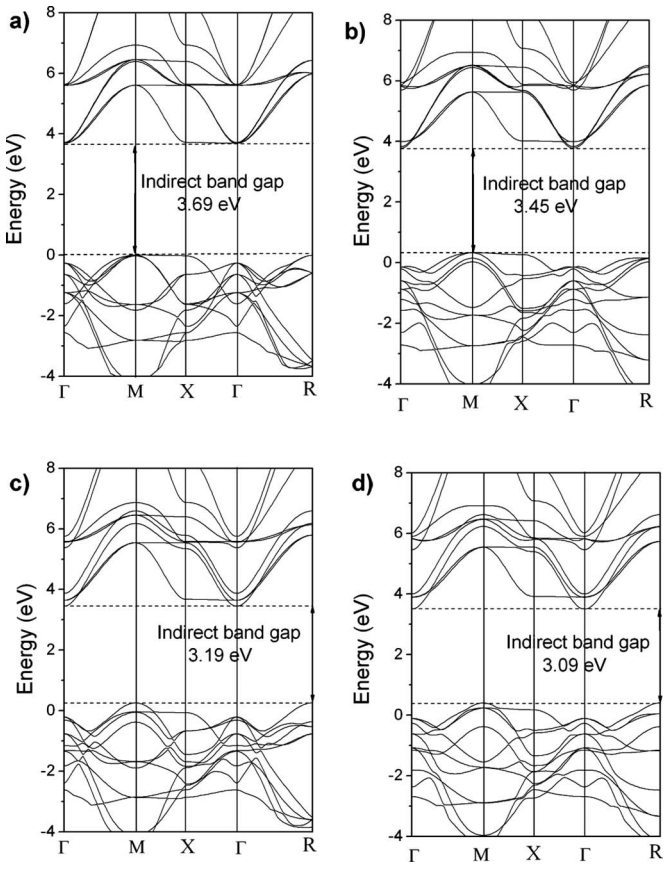

FIG. 5. Calculated energy band structure for (a) ST-o, (b) ST-f, (c) ST-m, and (d) ST-fm. The zero of the energy scale was set at the Fermi energy of ST-o.

Many other displacement tests were carried out. The results of these displacements were very similar to the results that will be presented. Although these results were quantitatively different, they did not change the focus of the models proposed herein.

Using these models, a detailed theoretical study was made of the band structure, atom-resolved projected DOS and electron density maps in ordered and asymmetric models.

Figure 5(a) depicts the calculated band structure of bulk ST-o. The top of the VB is at the *M* point and is very close to the *X* point. The bottom of the CB is at the Γ point. The minimal indirect gap between *M* and Γ is 3.69 eV, which is close to the experimental one deduced from the optical absorption edge, which was found to be 3.20 eV.

The calculated band structure of bulk ST-f is depicted in Fig. 5(b). The top of the VB is at the *M* point and the bottom of CB is at Γ, as in the case of ST-o. The indirect minimal gap between *M* and Γ is 3.45 eV.

The calculated band structures of ST-m and ST-fm are shown in Figs. 5(c) and 5(d), respectively. In both cases, the top of the VB is at the *R* point and the bottom of CB is at Γ. In the ST-m model, the indirect minimal gap between *R* and Γ is 3.19. The theoretical indirect gap of the ST-fm model was found to be 3.09 eV and represents the experimental disordered powders annealed at 673 and 723 K.

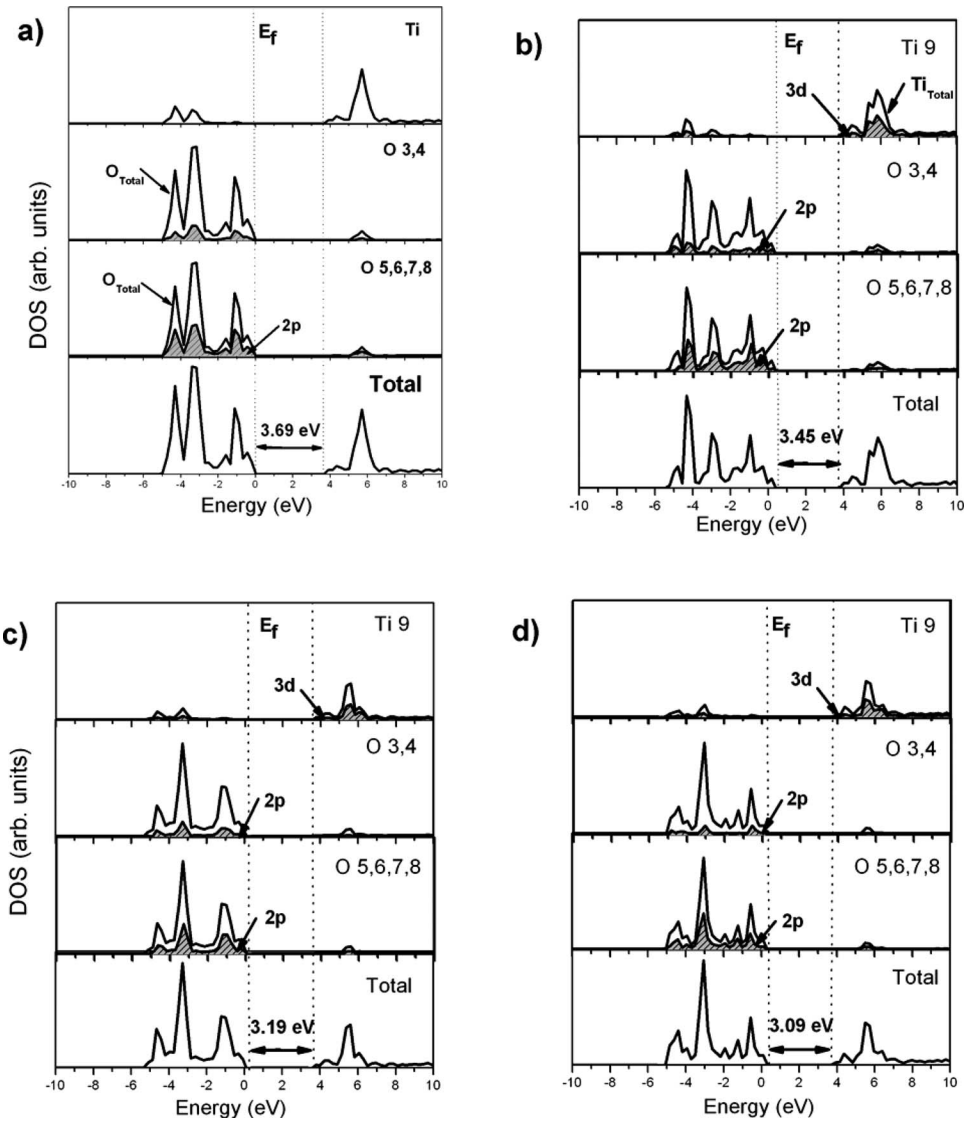

FIG. 6. Total and atom-projected DOS for the (a) ST-o, (b) ST-f, (c) ST-m, and ST-fm models.

These results confirm that our data are consistent with the interpretation that the exponential optical absorption edge and the optical band gap are controlled by the degree of structural disorder in the lattice of the ST powders (see Fig. 3). The theoretical analysis suggests that the network modifier lattice causes increased disorder in the lattice when compared to the network former lattice.

In the ST-o [Fig. 5(a)], the VBs from O ($2p_x$, $2p_y$, $2p_z$) atomic orbitals. These bands are separated by an indirect gap from the first CB, which derives from transition-metal titanium ($3d_{xy}$, $3d_{xz}$, $3d_{yz}$) atomic orbitals, designated as t_{2g} by comparison with the $[TiO_6]$ regular cluster. Above these six bands are four Ti ($3d_{x^2-y^2}$ and $3d_{z^2}$) character bands designated as e_g. For the dislocated models (ST-f, ST-m, and ST-fm), although the VB is globally constituted of O ($2p_x$, $2p_y$, $2p_z$) character states, the top mainly depends on the oxygen located at the center of the structure, O4 and O3 for the ST-f model and O5, O6, O7, and O8 for the ST-m and ST-fm models. The CB is composed of the $3d$ states of titanium, in an apparently random splitting of bands [Figs. 5(b)–5(d)].

The calculated total and atom-resolved projected DOSs of ST-o, ST-f, ST-m, and ST-fm are shown in Fig. 6, ranging from −10 eV below the top of the VB to 10 eV above. In the case of ST-o, the upper VB is predominately composed of the O ($2p$) states, equivalently distributed in the axial O3 and O4 oxygen atoms and O5, O6, O7, and O8 planar oxygen atoms of the structure [Fig. 6(a)]. In the case of ST-f [Fig. 6(b)], although the VB also comprises O ($2p$) states, the upper part, i.e., the new states, presents a strong O3, O4 character, the oxygen atom that loses its connection with Ti9 (Fig. 1). In the ST-m case [Fig. 6(c)], the upper part of VB comprises mainly the planar $2p$ oxygen states (O5, O6, O7 and O8). The ST-fm structure is analogous, proving that the network modifier creates a lift of degeneracy greater than that of the network former [Fig. 6(d)]. The CB is clearly made of the Ti ($3d$) states in the ordered and disordered structures. The Ti-O covalent bond creates a limited Ti ($3d$) contribution in the O ($2p$) region, as well as a weak O ($2p$) contribution to the Ti ($3d$) area.

The Sr ($5s$) states (not shown) are to be found in energies above −10 eV and more dispersed in the case of disordered models. These levels are weakly hybridized with oxygen levels in the ST-f model.

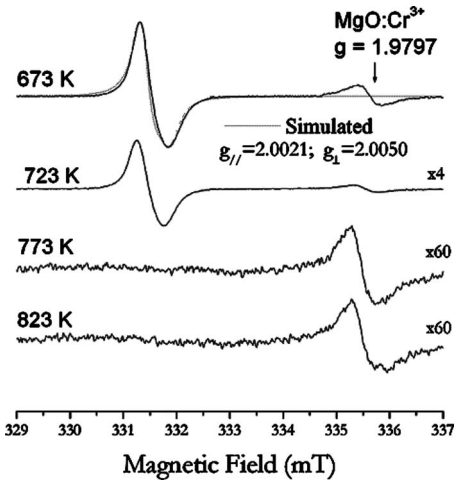

FIG. 7. Thermal dependent changes in the EPR spectrum of ST annealed at 673, 723, 773, and 823 K.

The degeneracy lift gives rise to new electronic levels in the VB and CB. Therefore, the distorted models (ST-f, ST-m, and ST-fm) can also be seen as a crystalline model like a Jahn–Teller distortion.[53]

The direct observation of oxygen vacancies is difficult, but spectroscopic studies of doped and annealed crystals indicate the presence of these vacancies.[54,55] EPR spectroscopy is an excellent tool for identifying and qualitatively monitoring complex oxygen vacancies that modify the electronic and ionic conductivities or grain boundary properties. Aliovalent acceptor dopants ($M^{\bullet}$ or $M^{\bullet\bullet}$) in strongly axially distorted surroundings were first detected and analyzed in ST (Refs. 56–58) $BaTiO_3$ (Ref. 59) and other perovskites in the 1960s.[60] Li *et al.*[61] correlated the emission of yellow PL with the $g \sim 1.96$ EPR signal of oxygen vacancies in ZnO nanostructures synthesized by different methods. The authors suggest that this signal is linked to deep or shallow donor concentration and green or yellow PL, depending on the depth of the level involved. Studies of visible luminescence in TiO_2 nanotubes and EPR spectra have revealed a strong signal at $g=2.0034$,[62] which is characteristic of single-electron-trapped oxygen vacancies ($V^{\bullet}$).[63]

Figure 7 shows the *X*-band EPR spectra of the ST powders annealed at 673, 723, 773, 823, and 1023 K and recorded at room temperature.

The ST powder annealed at 673 K presents an intense main feature and an asymmetric line. The spin-Hamiltonian parameters of the main contribution were estimated by comparing the room temperature spectrum to the spectra generated by computer simulation. Electrons are known to determine the transport properties, e.g., electrical conductivity, while no phenomena related to holes have been observed. This indicates that holes are almost trapped around defects.[64] The calculated values of $g_{\perp}=2.0050$ and $g_{\parallel}=2.0021$ are in accordance with an axial species.[62,63] The EPR technique only detects species that possess unpaired electrons, in this case, the $[TiO_5 \cdot V_O^{\bullet}]$ and $[SrO_{11} \cdot V_O^{\bullet}]$ complex clusters. The intensity of this line was reduced in samples annealed at 723 K and absent at 773 K, indicating that these complex clusters disappear when the structure is ordered.

The EPR spectra suggest that higher annealing heat reduces the singly ionized oxygen vacancies in disordered ST powders, creating electron-captured oxygen vacancies, according to the following equations, were Kröger–Vink notation is used:

$$[TiO_6]^x + [TiO_5 \cdot V_O^x] \rightarrow [TiO_6]' + [TiO_5 \cdot V_O], \quad (1)$$

$$[TiO_6]^x + [TiO_5 \cdot V_O] \rightarrow [TiO_6]' + [TiO_5 \cdot V_O^{\cdot}], \quad (2)$$

$$[SrO_{12}]^x + [SrO_{11} \cdot V_O^x] \rightarrow [SrO_{12}]' + [SrO_{11} \cdot V_O], \quad (3)$$

$$[SrO_{12}]^x + [SrO_{11} \cdot V_O] \rightarrow [SrO_{12}]' + [SrO_{11} \cdot V_O^{\cdot}], \quad (4)$$

where $[TiO_6]'$ or $[SrO_{12}]'$ are D′ donors, $[TiO_5 \cdot V_O^{\bullet}]$ or $[SrO_{11} \cdot V_O^{\bullet}]$ are donors/acceptors, and $[TiO_5 \cdot V_O^{\bullet\bullet}]$ and $[SrO_{11} \cdot V_O^{\bullet\bullet}]$ are $D^{\bullet}$ acceptors. We assume that charge redistribution may lead to electron-hole recombination of localized excitons.

Figure 8 depicts the electron density maps for the ST-o and ST-f models. To understand the density of charges, contour and surface plots were drawn of the electronic charge density calculated from two selected horizontal planes in the (0 0 0.25) and (0 0 0.75) planes containing Ti and O atoms.

An analysis of Fig. 8(a) clearly shows that the bond between Ti and O atoms has a covalent character due to hybridization between the O ($2p$) states and the Ti ($3d$) states. This behavior is represented by the homogenous distribution of the contour lines. Figure 8(b) presents an inhomogeneous distribution, indicated by contour lines which represent the declining interaction between the Ti and O4 atom due to the break of this bond. This charge gradient and the presence of the localized states provide a good condition for trapping of electrons (e') and holes ($h^{\bullet}$) during the excitation process. The recombination $e'/h^{\bullet}$ generates the polarons, favoring photoluminescent emission at room temperature in the visible region by disordered ST powders. The disordered structure presents a structural asymmetry that leads to differences of formal charge between clusters, suggesting polarization of the system.

Before the heat treatment reaches 773 K, the structure is composed of an aleatory mixture of $[TiO_5 \cdot V_O^x]$ and $[TiO_6]$ linked by strontium ions. These ionic materials are stable because of short-range and long-range repulsions between adjacent electron clouds. The existence or absence of order or disorder is determined by the balance between these short-range and long-range repulsions, which favor the ordered or disordered structure and may stabilize the disordered, intermediately ordered, or ordered structure.[65] Even in disordered structures, the short-range repulsions predominate $[TiO_5 \cdot V_O^x] \gg [TiO_6]$, resulting in a random disorder. Because of the electric dipolar interaction, which, in this case, is a long-range interaction, the effective field approximation can be applied to a model system in which a dielectrically soft local atomic configuration can be identified, albeit possibly distorted in the glassy phase (disordered).

This disorder is produced by clusters of different $[TiO_6]$ and $[TiO_5 \cdot V_O^x]$ coordinations, forming nano- and microentities whose size and order are determined by their temperature dependence. As the temperature increases, the stabiliza-

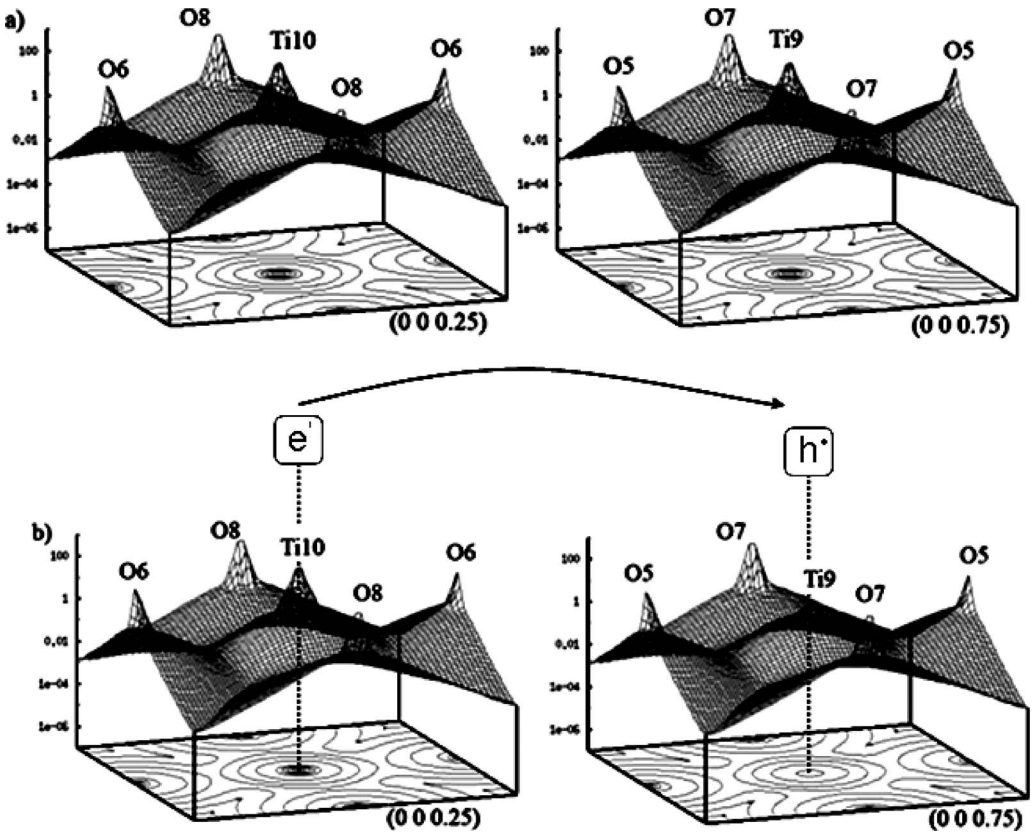

FIG. 8. Electron density maps of two horizontal planes of Ti–O: (a) ST-o model on the (0 0 0.25) (left) and (0 0 0.75) (right) planes; and (b) ST-f model, after displacement of the Ti atom, on the (0 0 0.25) (left) and (0 0 0.75) (right) planes. The ST-d model is used to speculate on the presence of the (e') and hole ($h^{\bullet}$).

tion forces associated with the polarization of the clusters as they are displaced become stronger than the short-range repulsive cluster-cluster interactions and the stable intermediate phase.

Figure 9(a) illustrates PL spectra recorded at room temperature for the ST powders heat treated at 673, 723, 773, 823, and 1023 K. The profile of the emission band is typical of a multiphonon process, i.e., a system in which relaxation occurs by several paths, involving the participation of numerous states within the band gap of the material. This behavior is related to the structural disorder of ST and indicates the presence of additional electronic levels in the forbidden band gap of the material.

The general aspect of the spectra is a broad band covering a large part of the visible spectra, from ~370 to 850 nm. As can be seen, the structurally disordered powder annealed at 673 K presents PL emission centered at 610 nm (green-yellow-light emission) and an intense PL emission centered at 550 nm (blue-green-light emission) when annealed at 723 K. When the crystallization process takes place at 773, 823, and 1023 K, PL emission is almost nonexistent. Hence, the interesting PL properties of structurally ordered-disordered ST powders lie within the range of 673–773 K and are governed by complex cluster vacancies. The very low PL emission in crystalline ST lies outside the scope of this paper.

For a better understanding of the PL properties and their dependence on the structural order-disorder of the lattice, the PL curves were analyzed by deconvolution PickFit.[66] Based on the Gaussian line broadening mechanism for luminescence processes, the fine features in the PL spectra of samples annealed at 673 and 723 K temperatures were deconvoluted, as shown in Fig. 9(b). The features extracted from the deconvolution curves and from the area under the curve of the respective transitions are listed in Table I.

We believe that the PL curves shown in Fig. 9 are composed of five PL components, which we have dubbed component violet (maximum below 438 nm), component blue (maximum below 488 nm), component green (maximum below 551 nm), component yellow (maximum below 623 nm), and component red (maximum below 710 nm) in allusion to the regions where the maxima of the components appear. We found that increasing the annealing temperature caused the structure of the ST powders to become more ordered, favoring the emission of bluish-green light (smaller wavelength) with higher energies. This bluish-green emission was very intense.

Quantum mechanical calculations of disordered $[TiO_6]$ and/or $[SrO_{12}]$ clusters indicate that localized states generated in the band gap reduce the gap energies. As the structural order increases, so does the gap energy. These observations confirm the fact that PL is directly associated with the localized states existing in the band gap and that the degree of order-disorder changes these localized states. The violet and blue emissions can be ascribed to shallow defects and the green, yellow, and red emissions to deep defects.

Each color therefore represents a different type of elec-

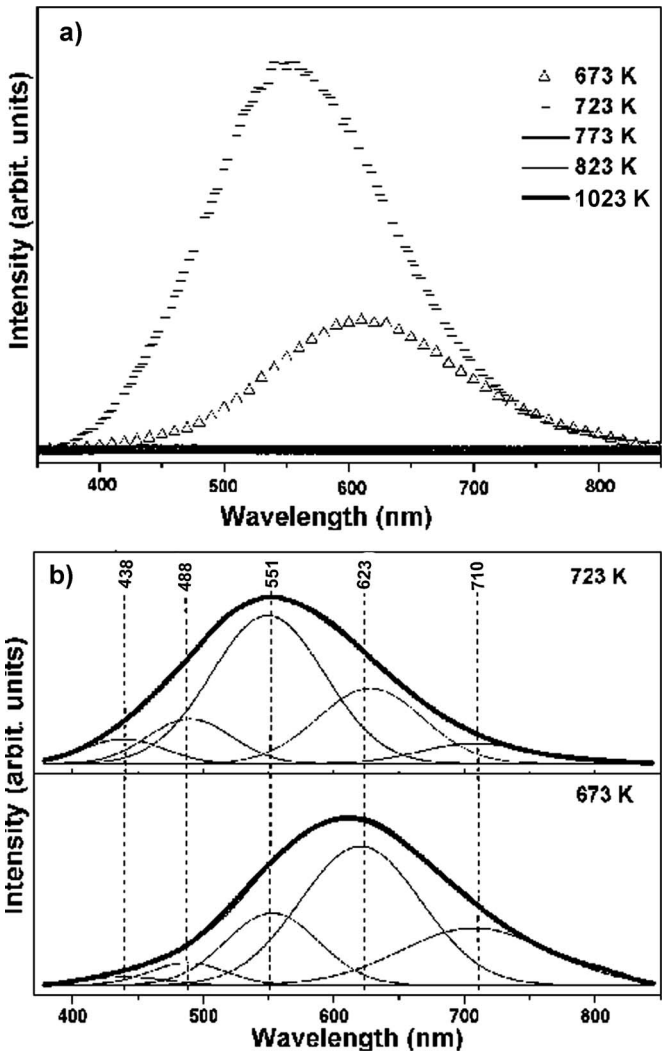

FIG. 9. (a) Room temperature PL spectra of ST powder samples annealed at 673, 723, 773, 823, and 1023 K for 2 h in an oxygen flow. The exciting wavelength was the 350.7 nm line of a krypton ion laser. (b) Deconvolution PickFit of the samples annealed at 673 and 723 K.

tronic transition and is associated with a specific structural arrangement. We attributed the increased disorder in the lattice to the presence of $[TiO_5 \cdot V_O^{\bullet\bullet}]$ and $[SrO_{11} \cdot V_O^{\bullet\bullet}]$ complex clusters, and these complex defects were inserted deeply in the band gap, leading to yellow-red PL emission. The $[TiO_5 \cdot V_O^{\bullet}]$ and $[SrO_{11} \cdot V_O^{\bullet}]$ complex clusters are linked to shallow defects in the band gap and lead to a more energetic PL emission (violet-blue-green light). As the order in the lattice increases, these complex vacancies disappear, as does the PL emission which is correlated to the vacancies.

TABLE I. The fitting parameters of the five Gaussian peaks. *T* =temperature of heat annealing; VC=violet component of PL; BC=blue component of PL; GC=green component of PL; YC=yellow component of PL; and RC=red component of PL.%

T	VC %[a] (438 nm)	BC %[a] (488 nm)	GC %[a] (551 nm)	YC %[a] (623 nm)	RC %[a] (710 nm)
673	2	5	20	49	24
723	6	12	51	24	7

[a]Obtained by dividing the area of each decomposed PL curves by the total PL area.

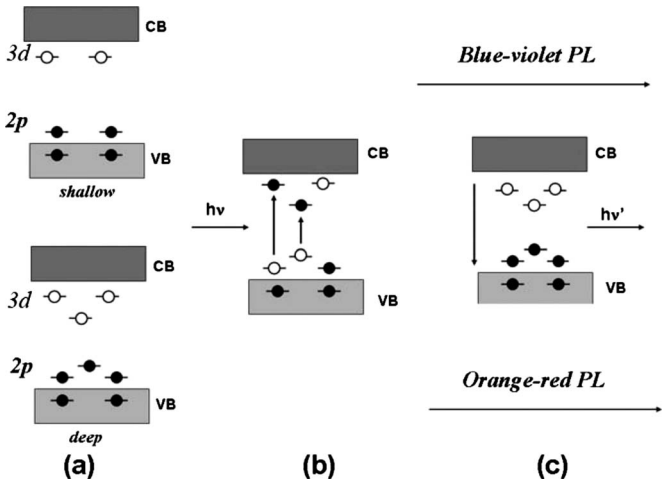

FIG. 10. Wide band model. (a) Before excitation, where D′ are donors and $D^{\bullet}$ are acceptors; (b) excitation formation of STE; (c) after excitation recombination of e^- and $h^{\bullet}$.

The intensity of PL emission depends mainly on the interaction between these complex clusters and the excitation wavelength. This interaction, which can be examined by means of time-resolved spectroscopy analyses, has already been investigated by several authors.[14–17]

In our model, the wild band model[67] illustrated in Fig. 10, the most important events occur before excitation, i.e., before the arrival of the photon. The deep and shallow oxygen complex clusters generate localized states in the band gap and inhomogeneous charge distribution in the cell, allowing the electrons to be trapped. The localized levels are energetically distributed, so that various energies are able to excite the trapped electrons.

In the complex, the $[TiO_6]'$ or $[SrO_{12}]'$ clusters act as electron donors, while the vacancy complex $[TiO_5 \cdot V_O^{\bullet}]$ or $[SrO_{11} \cdot V_O^{\bullet}]$ tends to trap electrons and/or holes and $[TiO_5 \cdot V_O^{\bullet\bullet}]$ or $[SrO_{11} \cdot V_O^{\bullet\bullet}]$ acts as an electron trap. After excitation of the photon, the recombination and decay process follows the several valid hypotheses presented in the literature.[14–17]

The present work shows that these complex clusters, which already exist in the ground state, facilitate the emission process leading to PL, i.e., to radiative recombination, as was confirmed by XANES and EPR experimental measurements and simulated by density functional calculations. Our ordered-disordered ST powders thus extrinsically possess the necessary structural condition for creating PL at room temperature. The ordered powders with quasiperfect structures do not allow for the creation of extrinsic defects and present very low PL emission at room temperature.

V. CONCLUSIONS

ST powders were synthesized by a soft chemical process and experimentally characterized by several complementary characterization techniques such as XRD, EPR spectroscopy, XANES spectroscopy, optical absorption, and PL spectroscopy.

The experimental XANES results of the disordered powders indicated that defects in the lattice are linked to structural defects composed of oxygen-deficient complex clusters of $[TiO_5 \cdot V_O^z]$ and $[SrO_{11} \cdot V_O^z]$. EPR spectroscopy confirmed the paramagnetic $[TiO_5 \cdot V_O^{\bullet}]$ and $[SrO_{11} \cdot V_O^{\bullet}]$ complex clusters having one unpaired ↑ electron.

First principles calculations based on the DFT at B3LYP level were used to interpret the formation of these complex clusters and the favorable conditions that give rise to PL emission. The electronic structures in four models representing the order and disorder in network former, network modifier, and network former and modifier models were examined in terms of band diagram, DOS, and electronic charges.

The calculations indicated that localized states generated in the band gap reduce the gap energies. As the structural order increases, so does the gap energy. These observations confirmed that PL is directly associated with the localized states existing in the band gap and that the degree of order-disorder changes these localized states. We found that an increased disorder in the lattice is associated with the presence of $[TiO_5 \cdot V_O^{\bullet\bullet}]$ and $[SrO_{11} \cdot V_O^{\bullet\bullet}]$ complex clusters and that these complex defects are inserted deeply in the band gap, leading to green-yellow-red PL emission. Thus, $[TiO_5 \cdot V_O^{\bullet}]$ and $[SrO_{11} \cdot V_O^{\bullet}]$ complex clusters are linked to shallow defects in the band gap and lead to stronger PL emission (violet-blue light). With increasing order in the lattice, these complex vacancies disappear and PL emission is very low.

Our ordered-disordered ST powders thus extrinsically possess the structural conditions for creating PL at room temperature. The ordered powders with quasiperfect structures do not allow for the creation of extrinsic defects and present very low PL emission at room temperature.

ACKNOWLEDGMENTS

This work was partially supported by the Brazilian research-financing institutions: FAPESP/CEPID, CNPq/PRONEX, and CAPES. Research partially performed at LNLS-National Laboratory of Synchrotron Light, Brazil.

[1] L. T. Canham, Appl. Phys. Lett. **57**, 1046 (1990).
[2] M. Capizzi and A. Frova, Phys. Rev. Lett. **25**, 1298 (1970).
[3] T. Hasegawa, M. Shirai, and K. Tanaka, J. Lumin. **87**, 1217 (2000).
[4] H. Suzuki, H. Bando, Y. Ootuka, I. H. Inoue, T. Yamamoto, K. Takahashi, and Y. Nishihara, J. Phys. Soc. Jpn. **65**, 1529 (1996).
[5] C. S. Koonce, M. L. Cohen, J. F. Schooley, W. R. Hosler, and E. R. Pfeiffer, Phys. Rev. **163**, 380 (1967).
[6] J. F. Schooley, W. R. Hosler, and M. L. Cohen, Phys. Rev. Lett. **12**, 474 (1964).
[7] O. N. Tufte and P. W. Chapman, Phys. Rev. **155**, 796 (1967).
[8] T. Feng, Phys. Rev. B **25**, 627 (1982).
[9] L. Grabner, Phys. Rev. **177**, 1315 (1969).
[10] M. Cardona, Phys. Rev. **140**, A651 (1965).
[11] G. A. Barbosa, R. S. Katiyar, and S. P. S. Porto, J. Opt. Soc. Am. **68**, 610 (1978).
[12] C. N. Berglund and H. J. Braun, Phys. Rev. **164**, 790 (1967).
[13] Y. T. Sihvonen, J. Appl. Phys. **38**, 4431 (1967).
[14] R. Leonelli and J. L. Brebner, Solid State Commun. **54**, 505 (1985).
[15] R. Leonelli and J. L. Brebner, Phys. Rev. B **33**, 8649 (1986).
[16] R. I. Eglitis, E. A. Kotomin, and G. Borstel, Eur. Phys. J. B **27**, 483 (2002).
[17] R. I. Eglitis, E. A. Kotomin, and G. Borstel, J. Phys.: Condens. Matter **14**, 3735 (2002).
[18] W. F. Zhang, Z. Yin, and M. S. Zhang, Appl. Phys. A: Mater. Sci. Process. **70**, 93 (2000).
[19] J. F. Meng, Y. B. Huang, W. F. Zhang, Z. L. Du, Z. Q. Zhu, and G. T. Zou, Phys. Lett. A **205**, 72 (1995).
[20] J. Yu, J. L. Sun, J. H. Chu, and D. Y. Tang, Appl. Phys. Lett. **77**, 2807 (2000).
[21] M. S. Zhang, Z. Yin, Q. Chen, W. F. Zhang, and W. C. Chen, Solid State Commun. **119**, 659 (2001).
[22] P. S. Pizani, H. C. Basso, F. Lanciotti, T. M. Boschi, F. M. Pontes, E. Longo, and E. R. Leite, Appl. Phys. Lett. **81**, 253 (2002).
[23] E. Orhan, J. A. Varela, A. Zenatti, M. F. C. Gurgel, F. M. Pontes, E. R. Leite, E. Longo, P. S. Pizani, A. Beltran, and J. Andres, Phys. Rev. B **71**, 085113 (2005).
[24] E. Longo, E. Orhan, F. M. Pontes, C. D. Pinheiro, E. R. Leite, J. A. Varela, P. S. Pizani, T. M. Boschi, F. Lanciotti, A. Beltran, and J. Andres, Phys. Rev. B **69**, 125115 (2004).
[25] F. M. Pontes, E. Longo, E. R. Leite, E. J. H. Lee, J. A. Varela, P. S. Pizani, C. E. M. Campos, F. Lanciotti, V. Mastelaro, and C. D. Pinheiro, Mater. Chem. Phys. **77**, 598 (2003).
[26] C. D. Pinheiro, E. Longo, E. R. Leite, F. M. Pontes, R. Magnani, J. A. Varela, P. S. Pizanni, T. M. Boschi, and F. Lanciotti, Appl. Phys. A: Mater. Sci. Process. **77**, 81 (2003).
[27] D. S. Kan, T. Terashima, R. Kanda, A. Masuno, K. Tanaka, S. C. Chu, H. Kan, A. Ishizumi, Y. Kanemitsu, Y. Shimakawa, and M. Takano, Nat. Mater. **4**, 816 (2005).
[28] W. F. Zhang, J. W. Tang, and J. H. Ye, Chem. Phys. Lett. **418**, 174 (2006).
[29] F. Chen, H. W. Liu, K. F. Wang, H. Yu, S. Dong, X. Y. Chen, X. P. Jiang, Z. F. Ren, and J. M. Liu, J. Phys.: Condens. Matter **17**, L467 (2005).
[30] M. S. Zhang, J. Yu, J. H. Chu, Q. Chen, and W. C. Chen, J. Mater. Process. Technol. **137**, 78 (2003).
[31] D. K. Schroder, *Semicondutor Material and Device Characterization* (Wiley, New York, 1990).
[32] S. R. Elliot, *Physics of Amorphous Materials* (Longman, London, 1990).
[33] M. Kastner, D. Adler, and H. Fritzsche, Phys. Rev. Lett. **37**, 1504 (1976).
[34] E. A. Davis, *Topics in Applied Physics: Physics of Amorphous Semiconductors* (Springer, Berlin, 1979).
[35] N. A. Bhat, K. S. Sangunni, and K. Rao, J. Non-Cryst. Solids **319**, 192 (2003).
[36] M. Kakihana and M. Yoshimura, Bull. Chem. Soc. Jpn. **72**, 1427 (1990).
[37] WINEPR SIMFONIA, version 1.25, Bruker Analytische Messtechnik GmbH (1996).
[38] E. Orhan, F. M. Pontes, C. D. Pinheiro, T. M. Boschi, E. R. Leite, P. S. Pizani, A. Beltran, J. Andres, J. A. Varela, and E. Longo, J. Solid State Chem. **177**, 3879 (2004).
[39] V. R. Saunders, R. Dovesi, C. Roetti, M. Causa, N. M. Harrison, C. M. Zicovich-Wilson, *CRISTAL98 User's manual* (University of Torino, Torino, 1998).
[40] C. T. Lee, W. T. Yang, and R. G. Parr, Phys. Rev. B **37**, 785 (1988).
[41] A. D. Becke, J. Chem. Phys. **98**, 5648 (1993).
[42] J. Muscat, A. Wander, and N. M. Harrison, Chem. Phys. Lett. **342**, 397 (2001).
[43] http://www.tcm.phy.cam.ac.uk/~mdt26/crystal.html.
[44] A. Kokalj, J. Mol. Graphics Modell. **17**, 176 (1999).
[45] R. V. Vedrinskii, V. L. Kraizman, A. A. Novakovich, P. V. Demekhin, and S. V. Urazhdin, J. Phys.: Condens. Matter **10**, 9561 (1998).
[46] V. Krayzman, I. Levin, J. C. Woicik, D. Yoder, and D. A. Fischer, Phys. Rev. B **74**, 224104 (2006).
[47] J. Xu, A. P. Wilkinson, and S. Pattanaik, Chem. Mater. **12**, 3321 (2000).
[48] B. Ravel and E. A. Stern, Physica B **209**, 316 (1995).
[49] F. Farges, J. Non-Cryst. Solids **204**, 53 (1996).
[50] D. L. Wood and J. Tauc, Phys. Rev. B **5**, 3144 (1972).
[51] S. de Lazaro, J. Milanez, A. T. de Figueiredo, V. M. Longo, V. R. Mastelaro, F. S. De Vicente, A. C. Hernandes, J. A. Varela, and E. Longo, Appl. Phys. Lett. **90**, 111904 (2007).
[52] E. A. Stern, Phys. Rev. Lett. **93**, 037601 (2004).
[53] S. Lenjer, O. F. Schirmer, H. Hesse, and T. W. Kool, Phys. Rev. B **66**, 165106 (2002).
[54] E. Auffray, P. Lecoq, M. Korzhik, A. Annenkov, O. Jarolimek, M. Nikl, S. Baccaro, A. Cecilia, M. Diemoz, and I. Dafinei, Nucl. Instrum. Methods Phys. Res. A **402**, 75 (1998).
[55] M. Nikl, P. Bohacek, E. Mihokova, M. Martini, F. Meinardi, A. Vedda, P. Fabeni, G. P. Pazzi, M. Kobayashi, M. Ishii, and Y. Usuki, J. Appl. Phys. **87**, 4243 (2000).
[56] E. S. Kirkpatrick, R. S. Rubins, and K. A. Muller, Phys. Rev. **135**, A86 (1964).

[57]R. A. Serway, W. Berlinger, K. A. Muller, and R. W. Collins, Phys. Rev. B **16**, 4761 (1977).
[58]R. Merkle and J. Maier, Phys. Chem. Chem. Phys. **5**, 2297 (2003).
[59]D. J. A. Gainon, J. Appl. Phys. **36**, 2325 (1965).
[60]K. A. Muller, J. Phys. (France) Lett. **42**, 551 (1981).
[61]D. Li, Y. H. Leung, A. B. Djurisic, Z. T. Liu, M. H. Xie, S. L. Shi, S. J. Xu, and W. K. Chan, Appl. Phys. Lett. **85**, 1601 (2004).
[62]L. Qian, Z. S. Jin, J. W. Zhang, Y. B. Huang, Z. J. Zhang, and Z. L. Du, Appl. Phys. A: Mater. Sci. Process. **80**, 1801 (2005).
[63]D. C. Cronemeyer, Phys. Rev. **113**, 1222 (1959).
[64]S. Mochizuki, F. Fujishiro, and S. Minami, J. Phys.: Condens. Matter **17**, 923 (2005).
[65]P. R. de Lucena, E. R. Leite, F. M. Pontes, E. Longo, P. S. Pizani, and J. A. Varela, J. Solid State Chem. **179**, 3997 (2006).
[66]T. Ding, W. T. Zheng, H. W. Tian, J. F. Zang, Z. D. Zhao, S. S. Yu, X. T. Li, F. L. Meng, Y. M. Wang, and X. G. Kong, Solid State Commun. **132**, 815 (2004).
[67]V. M. Longo, L. S. Cavalcante, A. T. de Figueiredo, L. P. S. Santos, E. Longo, J. A. Varela, J. R. Sambrano, C. A. Paskocimas, F. S. De Vicente, and A. C. Hernandes, Appl. Phys. Lett. **90**, 091906 (2007).